Steel and Composite Structures, *Vol. 26, No. 5 (2018) 573-582*
DOI: https://doi.org/10.12989/scs.2018.26.5.573

Development of a self-centering tension-only brace for seismic protection of frame structures

Pei Chi [1,2a], Tong Guo [1b], Yang Peng [3c], Dafu Cao [2d] and Jun Dong [*3]

[1] *Key Laboratory of Concrete and Prestressed Concrete Structures of the Ministry of Education, Southeast University, 2 Sipailou, Nanjing 210096, China*
[2] *College of Civil Science and Engineering, Yangzhou University, 88 South University Avenue, Yangzhou 225009, China*
[3] *College of Civil Engineering, Nanjing Tech University, 30 South Puzhu Road, Nanjing 211816, China*

(*Received August 23, 2017, Revised November 2, 2017, Accepted December 18, 2017*)

Abstract. This study develops and numerically verifies an innovative seismically resilient bracing system. The proposed self-centering tension-only brace (SC-TOB) is composed of a tensioning system to provide a self-centering response, a frictional device for energy dissipation, and a high-strength steel cable as a bracing element. It is considered to be an improvement over the traditional self-centering braces in terms of lightness, high bearing capacity, load relief, and double-elongation capacity. In this paper, the mechanics of the system are first described. Governing equations deduced from the developed analytical model to predict the behavior of the system are then provided. The results from a finite element validation confirm that the SC-TOB performs as analytically predicted. Key parameters including the activation displacement and load, the self-centering parameter, and equivalent viscous damping are investigated, and their influences on the system behavior are discussed. Finally, a design procedure considering controlled softening behavior is developed and illustrated through a design example.

Keywords: self-centering brace; tension-only brace; residual deformation; energy dissipation; pre-tension

1. Introduction

Braced frames are efficient and practical in resisting lateral loads; hence, they are among the most cost-effective systems in steel structures used for seismic application. Because of their high strength and stiffness, ordinary concentrically braced frames have shown a desirable level of performance during small earthquakes, but have not been considered suitable under strong earthquakes owing to the degrading hysteretic response of the bracing members and the limited deformation capacity. For regions with high seismic-hazard risk, braced systems with excellent energy dissipation and inelastic deformation capacities, such as special concentrically, eccentrically, and buckling-restrained braced frames, have been broadly employed to provide life safety and collapse prevention performance.

However, such conventional braced systems, although designed in accordance with modern building codes, are likely to produce large permanent residual deformations after moderate to severe seismic excitations. The socio-economic losses associated with residual deformations include (1) the costs of rehabilitation, including repair/demolition and relocation of the occupants; (2) an interruption of building function, particularly lifeline facilities such as hospitals, schools, and power facilities, which can severely impact people’s living and production, as well as rescue and relief efforts; and (3) a high collapse risk resulting from drift accumulations in the direction of the inelastic structural lean under P-Delta effects.

To address these drawbacks with traditional bracing systems and to work toward more resilient sustainable seismic structures, significant efforts have been devoted to novel bracing solutions to reduce or eliminate residual deformations. As a result, a self-centering energy-dissipative (SCED) brace, characterized by the use of pre-tensioned (PT) elements for re-centering capability and a friction mechanism for energy dissipation, was developed (Christopoulos *et al*. 2008). Experimental results confirmed the expected flag-shaped hysteresis behavior of the SCED brace within the target design drift without any structural damage. To demonstrate the complete seismic performance of a SCED-braced frame as designed, a shake table test on a three-story model was conducted (Erochko *et al*. 2013). Wiebe and Christopoulos (2011) proposed a new hysteretic model using Bézier curves to change the sharp stiffness transition of the SCED brace more gradually, and to modify the overestimated peak story accelerations calculated in the numerical analyses. Karavasilis *et al*. (2011) developed a nonlinear analytical model for a seismic analysis of structural systems with self-centering devices and supporting braces. To overcome the limitation of the self-centering capacity of SCED braces, two types of enhanced self-centering brace (SCB) configurations with multiple self-centering systems have been developed independently

∗Corresponding author, Professor, E-mail: dongjun@njtech.edu.cn
[a] Ph.D., E-mail: chipei@yzu.edu.cn
[b] Professor, E-mail: guotong@seu.edu.cn
[c] Assistant Professor, E-mail: yang.peng@njtech.edu.cn
[d] Professor, E-mail: dfcao@yzu.edu.cn

http://www.techno-press.org/?journal=scs&subpage=6
ISSN: 1229-9367 (Print), 1598-6233 (Online)

(Chou and Chen 2012, Erochko *et al*. 2014). The hysteretic responses and mechanics of steel frames equipped with these enhanced SCBs were also confirmed both experimentally and numerically (Chou *et al*. 2016). Introducing self-centering mechanisms in buckling-restrained brace (BRB) systems, Liu *et al*. (2012) developed a self-centering BRB (SC-BRB), which uses PT steel strands to provide a restoring force and BRB as the energy-dissipative component. However, the axial deformation capacity is limited owing to the poor elastic elongation of the steel strands. Zhou *et al*. (2014, 2015) proposed and experimentally investigated an improved SC-BRB using basalt fiber-reinforced polymer as PT elements, which achieves a stable and desirable flag-shaped hysteresis. A self-centering property can also be provided through pre-pressed disc springs, which has led to the development of a pre-pressed spring for a self-centering energy dissipation brace (Xu *et al*. 2016a, b). For higher self-centering capacity, the developed SCBs often consist of two or more sets of compressive steel bracing members. However, such members may not only reduce the reliability of the brace owing to complex configurations but also lead to excessive initial axial stiffness generally controlled by global buckling, which also has a negative influence on the seismic performance of the SCBs and their braced frames.

Alternatively, tension-only braces (TOBs) can be used in buildings located in low seismic intensity regions with advantages of lightness, high strength, slenderness, and specifically, buckling-free conditions. Frame structures braced with TOBs have a relatively longer fundamental period, which helps relieve the seismic forces induced in the structures, and consequently requires fewer materials to be used for the frame, thus saving on material costs. In light of this, substantial efforts have been made to investigate the feasibility of extending the applications of TOBs. Tang *et al*. (2016) focused on applying PT cable braces for controlling the lateral displacement of buildings. Zahrai and Mousavi (2016) proposed a new cable-pulley bracing system, which operates as a secondary load-resisting mechanism to improve the story drift distribution even for wide frames with large openings. Hou and Tagawa (2009),and Mousavi and Zahrai (2016), were interested in the use of pre-slacked wire rope/cable braces for a seismic retrofitting of steel moment frames. However, owing to their severe pinching hysteresis with undesirable energy dissipation, the current seismic codes prohibit the use of TOBs as sole bracings in high intensity regions (ASCE 7 2010, AISC 341 2010, Eurocode 8 2013). Nonetheless, their seismic performance can be improved by applying them in conjunction with various types of damping systems, which make them promising seismic-resilient bracings with respect to the significant advantages that they afford (Sorace and Terenzi 2012a, b, Kurata *et al*. 2012, Zahrai *et al*. 2017, Mousavi and Zahrai 2017).

In view of the potential benefits in the use of SCBs and TOBs, this study investigated an innovative flexible bracing system, referred to as a self-centering tension-only brace (SC-TOB), which integrates the concepts of TOB and SCB as proposed by Chi *et al*. (2016). The mechanics of the system as well as its overall concept are first explained. An analytical model that is able to predict the hysteresis behavior of the system was developed and subsequently verified through a finite element simulation. The effects of the key parameters including the activation displacement and load, self-centering, and equivalent viscous damping on the behavior of the system are investigated. The design procedure considering controlled softening behavior is also presented using a working example.

2. Analytical study of an SC-TOB

2.1 General mechanical description of the SC-TOB

The proposed SC-TOB, shown schematically in Fig. 1(a), is mainly composed of a tensioning system to provide self-centering capacity, a frictional device (FD) for energy dissipation, and a high-strength steel (HSS) cable as a bracing element with high bearing capacity.

A set of parallel-lay tendons (shown as a whole unit in Fig. 1 for illustrative purposes) pass around the frictionless pulley with one end anchored onto a sliding box (Fig. 1(b)),

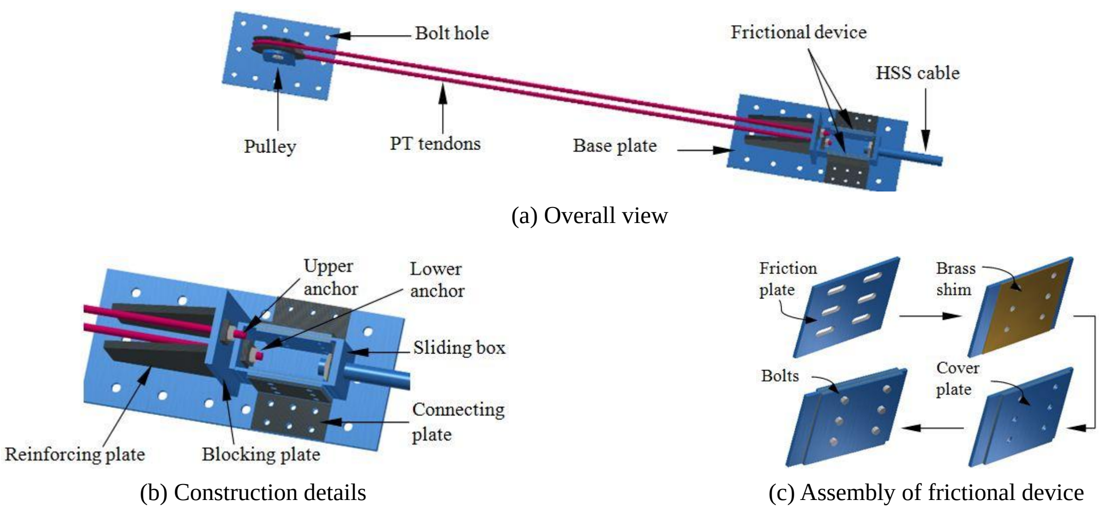

Fig. 1 Schematic of SC-TOB

which is allowed to move to the right, but is restricted from moving to the left by a blocking plate. Through a tensioning force applied to the tendons, and anchoring the other end onto the blocking plate, the sliding box is compressed tightly against the blocking plate. Thus, once the sliding box moves, the PT tendons are further elongated. This increases the tension in the PT tendons, and therefore produces additional restoring force to the system, providing a self-centering response. The pulley is employed to reduce the strain on the PT elements by half if the same elongation occurs, leading to a double-elongation capacity of a traditional SCB.

The FD, which is deemed to maintain stable energy dissipation, relies on a friction plate with long slotted holes (shown in Fig. 1(c)) sliding between two brass shims. The cover plates of the FD can be bolted to the base plate through a connecting plate.

The HSS cable is a bracing member with one end connected to the FD, and the other end attached to a connecting gusset plate. Using HSS, a significant stiffness reduction of the cable can be achieved without a failure in strength. Such reduction is desirable in seismic systems because it lengthens the fundamental period of structures equipped with a SC-TOB system, thereby mitigating their seismic response.

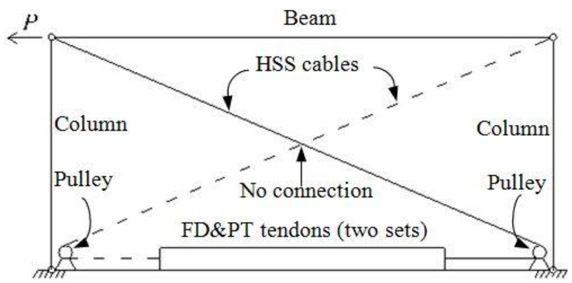

Fig. 2 Arrangement of SC-TOB

SC-TOBs can be installed in frame structures to dissipate the energy and provide self-centering capabilities. As shown in Fig. 2, HSS cable elements passing around frictionless pulleys placed at the top corner of the beam are attached to the brace connections, similar to traditional TOBs. However, the FD and PT tendons are arranged horizontally on the beam. For tension-only bracing, two SC-TOBs are required for each frame. In Fig. 2, the active HSS cable is represented through the solid lines, whereas the dotted lines denote the cable on stand-by for a load reversal.

2.2 Step-wise prediction of the SC-TOB response

The analytical model developed in Fig. 3 is used to illustrate the mechanics and force-displacement behavior of the SC-TOB system. The PT tendons, sliding box, and HSS cable are represented by three different springs with an axial stiffness labeled as K_t, K_b, and K_c, respectively, where $K_t = E_t A_t / l_t$, with E_t, A_t, and l_t being the Young's modulus, cross-sectional area, and original length of the PT tendons, respectively; and $K_c = E_c A_c / l_c$, with E_c, A_c, and l_c being the Young's modulus, cross-sectional area, and original length of the HSS cable, respectively. The blocking plate is depicted using a solid block. The left end of the system is pinned to a support, and a load P is applied to the end on its right side. The sliding box does not move until the increasing load P overcomes the sum of the pre-tension of the tendons, T_{t0}, and the frictional resistance of the FD, F. The activation load (corresponding to Event A in Fig. 3 (a)), P_a, is expressed as

$$P_a = T_{t,0} + F. \quad (1)$$

The full hysteretic behavior of the SC-TOB under cyclic loading can be divided into five key stages, as illustrated in Fig. 3.

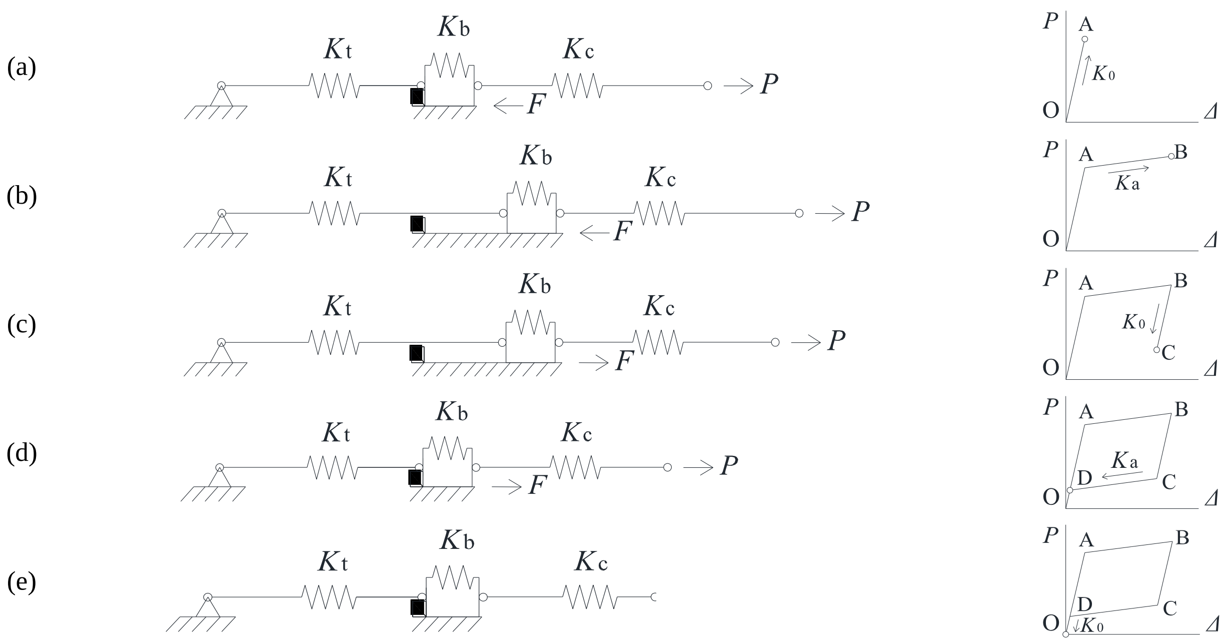

Fig. 3 Mechanics and hysteretic behavior of the SC-TOB

Table 1 Full solution of the SC-TOB hysteretic behavior

Stage	Axial stiffness	Tension in HSS cable	Tension in PT tendons
OA	K_0	$T_{c,OA} = K_0\Delta$	$T_{t,OA} = T_{t,0}$
AB	K_a	$T_{c,AB} = K_0\Delta_A + K_a(\Delta - \Delta_A)$	$T_{t,AB}$=$T_{c,AB} - F$
BC	K_0	$T_{c,BC} = K_0(\Delta_A - \Delta_B + \Delta) + K_a(\Delta_B - \Delta_A)$	$T_{t,BC}$=$T_{c,B} - F$
CD	K_a	$T_{c,CD} = K_0\Delta_D + K_a(\Delta - \Delta_D)$	$T_{t,CD}$=$T_{c,CD} + F$
DO	K_0	$T_{c,DO} = K_0\Delta$	$T_{t,DO} = T_{t,0}$

Stage O-A: In this stage (Fig. 3(a)), $P < P_a$, indicates that the sliding box remains stationary and can be regarded as a fixed support of the HSS cable. Thus, the initial axial stiffness of the SC-TOB, K_0, is solely determined by the axial stiffness of the HSS cable, i.e.

$$K_0 = K_c. \tag{2}$$

The tension in the HSS cable, T_c, is

$$T_c = K_c\delta_c = K_0\Delta, \tag{3}$$

where δ_c is the elongation of the HSS cable, and Δ is the end displacement of the SC-TOB.

Stage A-B: With continued loading, when $P \geq P_a$ (Fig. 3(b)), the sliding box starts to move, thereby activating the frictional dissipation mechanism. Meanwhile, a gap opens between the blocking plate and the sliding box, and increases up to its maximum value at Event B. In this stage, the axial stiffness of the system is significantly reduced to the post-activation stiffness, K_a, given by

$$K_a = \left(\frac{1}{K_t} + \frac{1}{K_b} + \frac{1}{K_c}\right)^{-1}. \tag{4}$$

Because $K_b \gg \max(K_t, K_c)$, the influence of K_b on K_a can be omitted. Consequently, Eq. (4) can be revised as

$$K_a = \left(\frac{1}{K_t} + \frac{1}{K_c}\right)^{-1}. \tag{5}$$

The tension in the HSS cable, T_c, is

$$T_c = P_a + K_a(\Delta - \Delta_a,) \tag{6}$$

where Δ_a is the end displacement of the SC-TOB at the onset of activation. The corresponding tension in the PT tendons, T_t, is

$$T_t = P - F. \tag{7}$$

Stage B-C: Upon unloading (Event B in Fig. 3(c)), the frictional force will first reduce gradually from F to zero, and then increase in the opposite direction to -F at Event C, with the difference between P_B and P_C being equal to $2F$. During this stage, the sliding box remains stationary once again, and hence, the axial stiffness of the SC-TOB is recovered to K_0, and the tension force of the PT tendons remains unchanged.

Stage C-D: With continued unloading, once a slippage of the sliding box is initiated to its original position (Event C in Fig. 3(d)), the energy dissipation mechanism is re-activated, and the stiffness of the SC-TOB is equal to K_a until the sliding box is back in contact against the blocking plate (gap closed at Event D). Because AD ∥ BC and P_B is $2F$ greater than P_C, P_D can be expressed as $P_D = P_A - 2F$. The area enclosed by the hysteresis loop of the system represents the energy that is dissipated during the cyclic loading.

Stage D-O: In this stage (Fig. 3(e)), the HSS cable works solely, and the stiffness of the brace is equal to K_c.

Based on the mechanical analysis above, the full solution of the SC-TOB hysteretic behavior is as summarized in Table 1.

2.3 Parametric analyses and discussions

2.3.1 Activation displacement and activation load

The activation point is a performance point associated with a key transition between the first two behavioral stages of the hysteresis of the SC-TOB system. It governs the conditions when the softening occurs and the energy-dissipative mechanism works. The location can be determined by computing the activation displacement, Δ_a, and the activation load, P_a.

Fig. 4 shows the configuration of a prototype frame structure equipped with SC-TOBs under a lateral load P, in which the stand-by cable for a stress reversal is not shown. Based on the geometry, Δ can be expressed as

$$\Delta = h\theta cos\alpha, \tag{8}$$

where h is the length of the column, θ is the inter-story

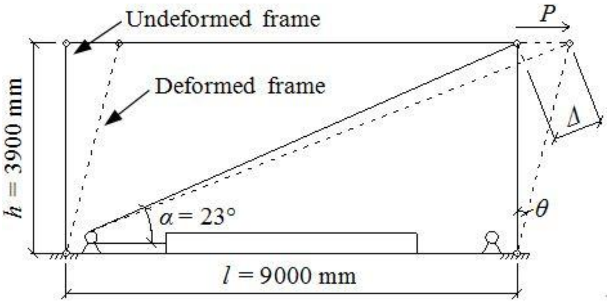

Fig. 4 Deformed configuration of the prototype SC-TOB frame

drift-angle, and α is the slope of the cable. It should be noted that, for a particular SC-TOB frame, h and α are fixed variables. Hence, Δ_a can be flexibly decided by specifying different values for θ, which may be selected from a wide range of values owing to the excellent elastic elongation capacity of HSS, unlike the limited values of mild steel. Once Δ_a is determined, P_a may be obtained by substituting Δ_a in Eq. (3), i.e.

$$P_a = K_0 h\theta cos\alpha \tag{9}$$

In this case, if $\theta = [\theta_e] = 0.4\%$ is selected, it indicates that activation occurs when the frame deforms to its allowable elastic inter-story drift angle, $[\theta_e]$ (GB 50011-2010 2010). Clearly, Δ_a and P_a are both displacement-related parameters. These allow the designer to select a smaller or greater θ to advance or delay the activation accordingly.

2.3.2 Self-centering capacity parameter

According to the mechanical analyses described in Section 2, it is deduced that a full self-centering capacity can only be achieved if point D (see Fig. 3) is located at the origin or above the horizontal axis, i.e.

$$P_D = P_A - 2F \geq 0. \tag{10}$$

Otherwise, the unloading curve would have an intersection with the horizontal axis, indicating that a residual deformation occurs. The self-centering capacity parameter, β, is defined as

$$\beta = \frac{T_{t,0}}{F}. \tag{11}$$

Substituting Eqs. (1) and (11) in Eq. (10) gives the full self-centering requirement as $\beta \geq 1$. One may obtain $T_{t,0}$ and F by substituting β in Eq. (1) as follows

$$T_{t,0} = \frac{\beta}{1+\beta} P_a, \tag{12}$$

$$F = \frac{1}{1+\beta} P_a. \tag{13}$$

As a key parameter describing the relative relationship between $T_{t,0}$ and F, β governs the overall performance of the SC-TOB in terms of the self-centering and energy-dissipative capacities. Theoretically, its optimal value should be $\beta = 1$ for the best energy dissipation under the premise of achieving full self-centering performance.

2.3.3 Equivalent viscous damping

Damping in actual structures is usually represented through the equivalent viscous damping. For a single-degree-of-freedom system, it can be defined by equating the energy dissipated in a vibration cycle and an equivalent viscous system (Chopra 2011). The damping ratio is calculated as

$$\zeta_{eq} = \frac{1}{4\pi} \frac{E_D}{E_{So}}, \tag{14}$$

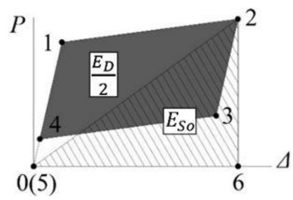

Fig. 5 Definition of E_D and E_{So}

where E_{So} and E_D are the strain energy and the energy dissipated in the SC-TOBs, respectively, and E_{So} is given by the area of triangle $\Delta 026$ indicated in Fig. 5, and is expressed as

$$E_{So} = S_{\Delta 026} = \frac{1}{2} P_2 \Delta_2. \tag{15}$$

Here, E_D is given by twice the area of polygon 1234 (two SC-TOBs for each bracing frame), and is expressed as

$$\begin{aligned} E_D &= 2S_{1234} = 2(S_{0126} - S_{04326}) \\ &= 2\Big(\frac{1}{2}\sum_{i=0}^{1}(P_{i+1}+P_i)(\Delta_{i+1}-\Delta_i) \\ &\quad -\frac{1}{2}\sum_{i=2}^{4}(P_{i+1}+P_i)(\Delta_i-\Delta_{i+1})\Big). \end{aligned} \tag{16}$$

Substituting Eqs. (15) and (16) in Eq. (14), ζ_{eq} is rewritten as

$$\zeta_{eq} = \frac{\sum_{i=0}^{1}(P_{i+1}+P_i)(\Delta_{i+1}-\Delta_i) - \sum_{i=2}^{4}(P_{i+1}+P_i)(\Delta_i-\Delta_{i+1})}{2\pi P_2 \Delta_2}. \tag{17}$$

3. Finite element simulation and validation

3.1 Finite element simulation

To simulate the hysteretic response of the SC-TOB, the 3D finite element (FE) model shown in Fig. 6 was developed using the computer program ABAQUS (Dassault Systems 2010).

All metal plates were modeled using eight-node solid elements with incompatible modes, C3D8I, which is suitable for dealing with “hard contact” behaviors, such as friction and relative sliding, as involved herein. An elasto-plastic law with the von Mises yielding criterion was specified for these metal plates, as shown in Fig. 7(a). The material selected for the PT tendons was aramid fiber-reinforced polymer (AFRP), and the principle of material selection is as described in Section 5. Both the HSS cable and the PT tendons were modeled using a two-node truss element, T3D2, with only linearly elastic properties, as shown in Fig. 7(b). The anchor plates for the HSS cable and the PT tendons were modeled using analytical rigid parts, which are un-deformable and cannot be meshed, to assure that tensile forces from the truss elements can be transferred uniformly to the contacting surfaces.

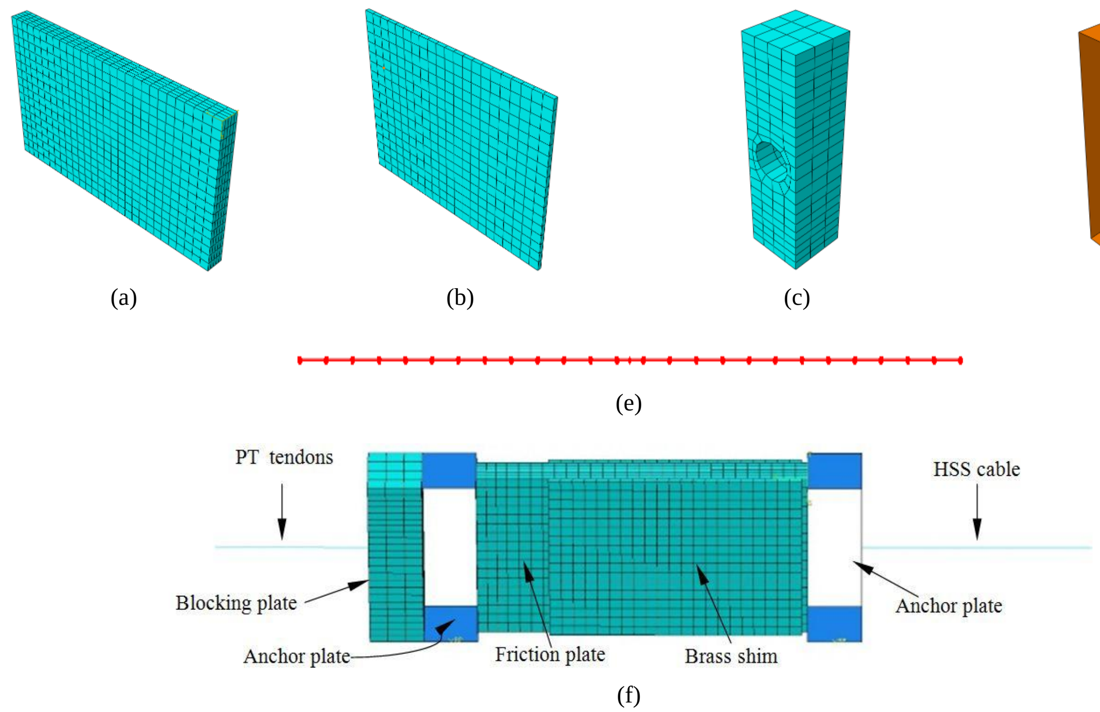

Fig. 6 Finite element model details: (a) friction plate; (b) brass shim; (c) blocking plate; (d) anchor plate; (e) HSS cable and PT tendons; and (f) assembly model for the SC-TOB

Fig. 7 Constitutive models

Tie constraints were defined between the contacting surfaces, namely, the PT tendons, anchor plate for the PT tendons, friction plate, anchor plate for the HSS cable, and HSS cable such that no relative motion occurred among them. A hard contact interaction with "finite sliding" was applied to the contact surfaces between the blocking plate and the anchor plate for the PT tendons in order to model their gap opening and closing behaviors under cyclic loading.

The FD was modeled as one friction plate (with an equivalent stiffness of the sliding box) sandwiched by two brass shims to decrease the computational scale. The Coulomb friction formulation technique was chosen for the interaction, specifying a constant coefficient of friction, μ_{FE}. The clamping force, N_F, which is applied to produce the friction force, can be computed as

$$N_F = F/n_{FE}\mu_{FE},$$

where n_{FE} is the number of friction surfaces in the model. Because n_{FE} was reduced to half of the actual number, μ_{FE} should be assumed as twice the actual value to ensure that F represented in the model agrees with the actual conditions. For each surface-to-surface contact definition, the master surface and the slave surface must be carefully selected in terms of the geometry, stiffness, and mesh fineness.

The required pre-tension in the PT tendons was applied by enforcing the pin support, which was assigned to the free end of the PT tendons, to produce a certain displacement, $\Delta_{t,0}$

$$\Delta_{t,0} = \frac{T_{t,0}}{K_t}. \tag{18}$$

The initial elongation of the PT tendons induced by the pre-tension, $\delta_{t,0}$, is equal to $\Delta_{t,0}$.

The FE model geometry almost replicates the analytical model geometry, except that the FD was modeled in a simplified manner, as previously mentioned. The dimensions

Table 2 Parameters of the FE prototype model

PT tendons					Friction plate				
d_t, mm	$l_{t,0}$, mm	f_t, MPa	E_t, GPa	$\delta_{t,0}, mm$	b_f, mm	d_f, mm	l_f, mm	f_f, MPa	E_f, GPa
35	10 000	2267	73	105	340	40	550	295	206
Brass shim					HSS cable				μ_{FE}
b_b, mm	d_b, mm	l_b, mm	E_b, GPa	σ_b, MPa	d_c, mm	$l_{c,0}$, mm	f_c, MPa	E_c, GPa	--
340	8	420	97	3.72	80	10 000	835	200	0.66

*where d_t, $l_{t,0}$, f_t, E_t, and $\delta_{t,0}$ are the diameter, length, tensile strength, Young's modulus, and initial elongation of the PT tendons; b_f, d_f, l_f, f_f, and E_f are the width, thickness, length, tensile strength, and Young's modulus of the friction plate; b_b, d_b, l_b, E_b, and σ_b are the width, thickness, length, Young's modulus, and clamping stress of the brass shims; d_c, $l_{c,0}$, f_c, and E_c are the diameter, length, tensile strength, and Young's modulus of the HSS cable, respectively; and μ_{FE} is the coefficient of friction between the steel and brass used in the model

dimensions of the metal plates were selected according to their effective areas by omitting all holes for simplification. A round hole was cut in the blocking plate, allowing the PT tendons to pass through and be connected to their anchor plate. The key parameters selected for the prototype model are listed in Table 2.

3.2 Finite element simulation validation

The force-displacement curves are plotted in Fig. 8 based on the FE analyses (parameters listed in Table 2) along with the analytical curves of both the HSS cable and PT tendons under monotonic displacement loading, among which the the cable curves represent the overall behavior of the SC-TOB system. It is shown that the tension in the PT tendons remains constant until the brace reaches its activation displacement, and then slowly increases. The curves for the cable and PT tendons are parallel after activation, indicating that the tensions in these two components increase at the same rate, where the difference is equal to the frictional resistance F. A slight error can be observed in Fig. 8 in that the post-activation stiffness of the system obtained from the analytical prediction is slightly greater than that obtained from the FE model, which is caused by the omission of the stiffness of the friction plate (see Eqs. (4) and (5)). Nevertheless, the FE model can trace the nonlinear behaviors of

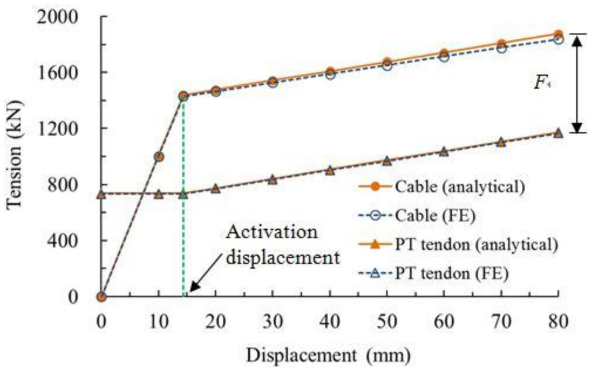

Fig. 8 Comparison of FE and analytical behaviors

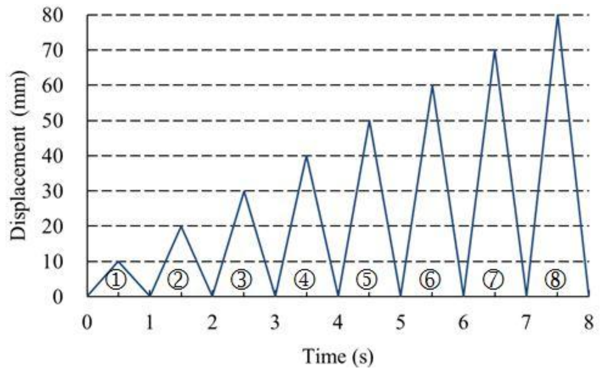

Fig. 9 Loading sequence

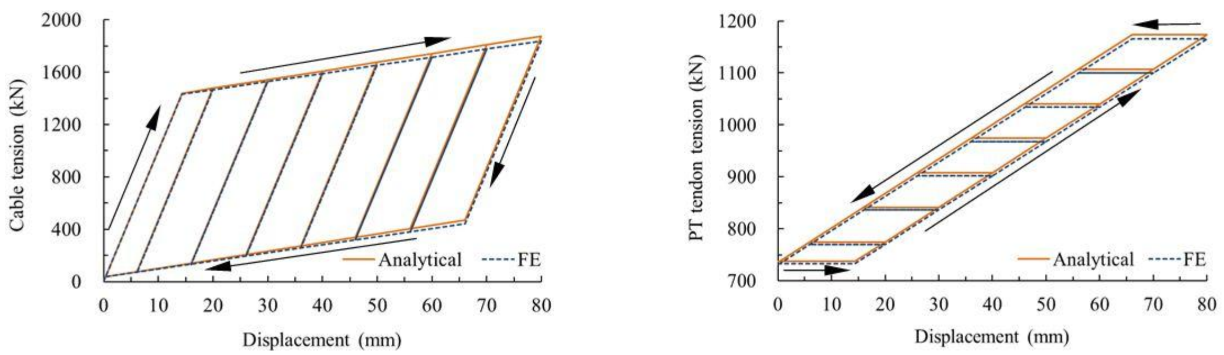

(a) HSS cable

(b) PT tendons

Fig. 10 Hysteretic responses of the SC-TOB both the cable and PT tendons with the desirable accuracy, and in particular, the activation displacement is captured precisely because a sufficiently small time increment of the analysis step is specified.

To validate the overall hysteretic response of the SC-TOB under cyclic loading, an FE simulation was conducted on the same model. The axial displacement applied to the HSS cable was used as a controlling parameter following the loading protocol, as specified in Fig. 9. Eight loading loops having peak values increasing from 10 to 80 mm at 10 mm intervals are also labeled, in which an 80 mm displacement corresponds to a 2.23% inter-story drift in the prototype structure, as shown in Fig. 4. The variations in tension in the HSS cable and PT tendons with the axial displacement are described in Fig. 10, where the arrows indicate the force path under the eighth loading loop. The FE results are in reasonably good agreement with corresponding analytical results. Both the cable and PT tendons exhibit a flag-shaped hysteresis without a residual deformation, i.e., a full self-centering capacity is achieved. For the first loading loop (peak displacement within 10 mm), the curves pertaining to loading and unloading appear to overlap, indicating that no energy was dissipated, whereas from the second loading loop onward, the hysteresis loops grow, and increasing energy is dissipated with the displacement. Overall, the results presented in Fig. 10 confirm the hysteretic performance of the SC-TOB system as predicted.

4. Design procedure of the SC-TOB considering controlled softening behavior

4.1 Softening coefficient of stiffness

The softening coefficient of stiffness of the SC-TOB system, α, is defined as the ratio of the post-activation stiffness, K_a, to the initial axial stiffness, K_0, namely

$$\alpha = \frac{K_a}{K_0}. \tag{19}$$

Unlike the similar post-yield stiffness ratio for conventional bracings such as a BRB, which is basically invariable owing to the inherent properties of the materials, α can be selected from a wide range of values by changing the material and length of the PT tendons to achieve a controlled post-activation stiffness. Hence, it is a unique parameter with regard to the controlled softening behavior of the SC-TOB, and should be taken into account in the design.

Substituting K_a from Eq. (5) in Eq. (19), the relationship between K_c (equal to $E_c A_c / l_c$) and K_t (equal to $E_t A_t / l_t$) is established, and can be expressed as

$$\frac{E_c A_c}{l_c} = \frac{1-\alpha}{\alpha}\frac{E_t A_t}{l_t}. \tag{20}$$

Substituting P_a from Eq. (13) and K_a from Eq. (19) in Eq. (6), the ultimate tension in the HSS cable, $T_{c,u}$, can be expressed as $T_{c,u} = (1+\beta)F + \alpha\frac{(1+\beta)F}{\Delta_a}(\Delta_u - \Delta_a)$, where Δ_u is the ultimate displacement of the end of the HSS cable. Consequently, the required area of the HSS cable, A_c, is

$$A_c \geq \frac{T_{c,u}}{f_c} = \frac{(1+\beta)F + \alpha\frac{(1+\beta)F}{\Delta_a}(\Delta_u - \Delta_a)}{f_c}. \tag{21}$$

According to Eq. (7), the ultimate tension in the PT tendons, $T_{t,u}$, is expressed as $T_{t,u} = T_{c,u} - F$, and thus the required area of the PT tendons, A_t, is

$$A_t \geq \frac{T_{t,u}}{f_t} = \frac{\beta F + \alpha\frac{(1+\beta)F}{\Delta_a}(\Delta_u - \Delta_a)}{f_t} \tag{22}$$

Substituting Eq. (22) in Eq. (20), the equation governing the fundamental parameters of the SC-TOB with emphasis on the controlled softening behavior is obtained as

$$\frac{E_c A_c}{l_c} \geq \frac{1-\alpha}{\alpha}\frac{E_t F\left[\beta + \alpha(1+\beta)\frac{\Delta_u - \Delta_a}{\Delta_a}\right]}{f_t l_t}. \tag{23}$$

4.2 Design procedure

The step-by-step design procedure for the SC-TOB system considering the controlled softening behavior is summarized as follows:

(1) Conduct an elasto-static analysis on an HSS cable braced frame under frequently occurred earthquakes to select the appropriate grade of strength for the HSS cable, and initially determine the cross-sectional area, A_c, according to the displacement requirement of the design code. Make sure that all HSS cables always remain elastic.
(2) Calculate the activation load, P_a, based on Eq. (9), at a preferred inter-story drift angle, θ.
(3) Determine the initial pre-tension of the tendons, T_{t0}, and the frictional resistance, F, based on Eqs. (12) and (13), respectively, after selecting an appropriate self-centering capacity parameter, β.
(4) Select a range of the softening coefficient of stiffness, α, as needed, and then determine the material and length for the PT tendons based on Eq. (23) after computing the ultimate displacement of the HSS cable, Δ_u, given by Eq. (8).
(5) Determine the cross-sectional area of the PT tendons, A_t, based on Eq. (22).
(6) Calculate α based on Eq. (20).
(7) Check whether A_c conforms to Eq. (21). Otherwise, go back to Step 1 using a larger A_c or f_c, or both.
(8) Calculate the initial elongation of the PT tendons, $\delta_{t,0}$, equal to $\Delta_{t,0}$, which is given by Eq. (18).

4.3 Design example

In this section, a design example of the SC-TOB is given following the proposed design procedure, along with an explanation on how the parameters listed in Table 2 are involved.

(1) Conduct an elasto-static analysis on an HSS cable braced frame under frequently occurred earthquakes, and select an HSS cable with A_c = 5024 mm^2 (diameter d_c = 80 mm), $f_c = 835$ MPa, $E_c = 200$ GPa, and $l_c = 10\,000$ mm.

(2) Select $\theta = 0.4\%$. From Eq. (9), the activation load, P_a, is calculated as 1438.98 kN.

(3) Select $\beta = 1.05$. Using Eqs. (12) and (13), the initial pre-tension of the tendons, $T_{t,0}$, and the frictional resistance, F, are computed as $T_{t,0} = 737.04$ and $F = 701.94$ kN, respectively.

(4) Because BRBs are prone to damage concentration over the structure height owing to their low post-yield stiffness ratio of between 1 and 5% (Tremblay *et al*. 2008, Chou *et al*. 2014), the softening coefficient of stiffness, α, is expected to be larger. However, too large a ratio may overload the brace connections and adjacent structural members (Qiu and Zhu 2016). Hence, α, which needs more discussion in future research, is considered herein to be $5\% \leq \alpha \leq 10\%$. From Eq. (8), after selecting the ultimate inter-story drift angle $\theta_u = 2\%$, the ultimate displacement of the HSS cable, Δ_u, is calculated as 71.60 mm. Select the length of the PT tendons as $10\,000$ mm. It can be deduced from Eq. (23) that the range for the ratio of the Young's modulus, E_t, to the tensile strength, f_t, of the PT tendons is $\frac{E_t}{f_t} \leq 85$. Hence, aramid fiber Technora-T200 (the published properties of which are $E_t = 73$ GPa and $f_t = 2.27$ GPa) was selected as PT tendon material.

(5) From Eq. (22), the cross-sectional area of the PT tendons, A_t, should be greater than $451\ \mathrm{mm}^2$. Select $A_t = 961\ \mathrm{mm}^2$ (diameter $d_t = 35$ mm).

(6) Based on Eq. (20), the softening coefficient of stiffness, α, is finally determined to be 6.53%.

(7) Use Eq. (21) to check A_c. Here, $A_c = 5024\ \mathrm{mm}^2 > \frac{T_{c,u}}{f_c} = 2260\ \mathrm{mm}^2$. This result indicates that for an HSS cable, the cross-sectional area initially determined in Step 1 is generally sufficient to resist the ultimate load. Basically, A_c is controlled based on the deformation requirement of the braced system instead of the strength requirement itself.

(8) According to Eq. (18), the initial elongation needed for the pre-tension of the tendons, $\delta_{t,0}$, is calculated as 105 mm.

5. Conclusions

An innovative, self-centering tension-only brace (SC-TOB) that combines post-tensioned tendons to provide a self-centering response, a friction device to dissipate seismic energy, and HSS cables as bracing elements was presented and investigated both analytically and numerically. The following conclusions can be drawn from this study:

- The mechanics of the SC-TOB system along with a concrete demonstration were illustrated. The basic equations that govern the cyclic behavior of the system were deduced from the developed analytical model. Key parameters including the activation displacement and load, self-centering parameter, and equivalent viscous damping were investigated, and their influence on the performances of the bracing system was discussed.
- The FE model accurately predicted the response of the SC-TOB in terms of variations in tension in an HSS cable and PT tendons under monotonic and cyclic loading. In particular, the activation behavior was captured precisely as long as a sufficiently small time incrementation of the analysis step was specified. However, an acceptable error between the FE and analytical results was observed, which was caused by an omission of the stiffness of the friction plate while conducting the analytical calculations. Basically, the FE validations confirmed that the SC-TOB performed as analytically predicted.
- The design procedure considering the controlled softening behavior, represented by the softening coefficient of the stiffness, α, was developed. A working example with a specified range of α was presented in detail to illustrate its practical application. However, α needs more investigation in future research.

Finally, it must be clarified that this work is primarily a study on the behavior of the SC-TOB system. Moreover, although an explicit FE model is deemed to be sufficiently accurate to confirm the findings, experimental studies are necessarily required, especially for practical concerns such as anchorage and placement of PT tendons around the pulley, for further verification and investigation.

Acknowledgments

The support from the National Natural Science Foundation of China (Grants No. 51708482 and 51578478) and China Postdoctoral Science Foundation (Grant No. 2017M621593) is gratefully acknowledged.

References

AISC 341 (2010), Seismic provisions for structural steel buildings, American Institute of steel construction; Chicago, IL, USA.

ASCE 7 (2010), Minimum design loads for buildings and other structures, American Society of Civil Engineers; Reston, VA, USA.

Chi, P., Dong, J., Peng, Y. and Liew, J.Y.R. (2016), "Theoretical and numerical study on an innovative self-centering energy-dissipative tension-brace system", *J. Vib. Shock*., **35**(21), 171-176. [In Chinese]

Chopra, A.K. (2011), *Dynamics of Structures*: *Theory and Applications to Earthquake Engineering*, (4th Edition), Prentice Hall, Upper Saddle River, NJ, USA.

Chou, C.C. and Chen, Y.C. (2012), "Development and seismic performance of steel dual-core self-centering braces", *Proceedings of the 15th World Conference on Earthquake Engineering*, Lisbon, Portugal, September.

Chou, C.C., Chen, Y.C., Pham, D.H. and Truong, V.M. (2014), "Steel braced frames with dual-core SCBs and sandwiched BRBs: Mechanics, modeling and seismic demands", *Eng. Struct.*, **72**, 26-40.

Chou, C.C., Wu, T.H., Beato, A.R.O., Chung, P.T. and Chen, Y.C. (2016), "Seismic design and tests of a full-scale one-story one-bay steel frame with a dual-core self-centering brace", *Eng. Struct.*, **111**, 435-450.

Christopoulos, C., Tremblay, R., Kim, H.J. and Lacerte, M. (2008), "Self-centering energy dissipative bracing system for the seismic resistance of structures: Development and validation", *J. Struct. Eng.*, **134**(1), 96-107.

Dassault Systems (2010), Abaqus User's Manual, (Version 6.10), Dassault Systemes Simulia Corp., Providence, RI, USA.

Erochko, J., Christopoulos, C. and Tremblay, R. (2014), "Design and testing of an enhanced-elongation telescoping self-centering energy-dissipative brace", *J. Struct. Eng.*, **141**(6), 04014163.

Erochko, J., Christopoulos, C., Tremblay, R. and Kim, H.J. (2013), "Shake table testing and numerical simulation of a self-centering energy dissipative braced frame", *Earthq. Eng. Struct. Dyn.*, **42**, 1617-1635.

Eurocode 8 (2005), Design of structures for earthquake resistance, European Committee for Standardization; Brussels, Belgium.

GB 50011-2010 (2010), Code for seismic design of buildings, Ministry of Housing and Urban-Rural Development of China; Beijing, China.

Hou, X.G. and Tagawa, H. (2009), "Displacement-restraint bracing for seismic retrofit of steel moment frames", *J. Constr. Steel Res.*, **65**(5), 1096-1104.

Karavasilis, T.L., Blakeborough, T. and Williams, M.S. (2011), "Development of nonlinear analytical model and seismic analyses of a steel frame with self-centering devices and viscoelastic dampers", *Comput. Struct.*, **89**(11-12), 1232-1240.

Kurata, M., Leon, R.T. and Desroches, R. (2012), "Rapid seismic rehabilitation strategy: Concept and testing of cable bracing with couples resisting damper", *J. Struct. Eng.*, **138**(3), 354-362.

Liu, L., Wu, B., Li, W. and Zhao, J.X. (2012), "Cyclic tests of novel self-centering buckling-restrained brace", *J. Southeast Univ.*, **42**(3), 536-541. [In Chinese]

Mousavi, S.A. and Zahrai, S.M. (2016), "Contribution of pre-slacked cable braces to dynamic stability of non-ductile frames; An analytical study", *Eng. Struct.*, **117**, 305-320.

Mousavi, S.A. and Zahrai, S.M. (2017), "Slack free connections to improve seismic behavior of tension-only braces: An experimental and analytical study", *Eng. Struct.*, **136**, 54-67.

Qiu, C.X. and Zhu, S.Y. (2016), "High-mode effects on seismic performance of multi-story self-centering braced steel frames", *J. Constr. Steel Res.*, **119**, 133-143.

Sorace, S. and Terenzi, G. (2012a), "The damped cable system for seismic protection of frame structures – Part I: General concepts, testing and modeling", *Earthq. Eng. Struct. Dyn.*, **41**(5), 915-928.

Sorace, S. and Terenzi, G. (2012b), "The damped cable system for seismic protection of frame structures – Part II: Design and application", *Earthq. Eng. Struct. Dyn.*, **41**(5), 929-947.

Tang, B.J., Zhang, F.X., Wang, Y. and Wang, F. (2016), "Effect of pre-stressed cable on pre-stressed mega-braced steel frame", *Struct. Eng. Mech., Int. J.*, **59**(2), 327-341.

Tremblay, R., Lacerte, M. and Christopoulos, C. (2008), "Seismic response of multistory buildings with self-centering energy dissipative steel braces", *J. Struct. Eng.*, **134**(1), 108-120.

Wiebe, L. and Christopoulos, C. (2011), "Using Bézier curves to model gradual stiffness transitions in nonlinear elements: application to self-centering systems", *Earthq. Eng. Struct. Dyn.*, **40**(14), 1535-1552.

Xu, L.H., Fan, X.W. and Li, Z.X. (2016a), "Development and experimental verification of a pre-pressed spring self-centering energy dissipation brace", *Eng. Struct.*, **127**, 49-61.

Xu, L.H., Fan, X.W., Lu, D.C. and Li, Z.X. (2016b), "Hysteretic behavior studies of self-centering energy dissipation bracing system", *Steel Comp. Struct., Int. J.*, **20**(6), 1205-1219.

Zahrai, S.M. and Mousavi, S.A. (2016), "Cable-pulley brace to improve story drift distribution of MRFs with large openings", *Steel Comp. Struct., Int. J.*, **21**(4), 863-882.

Zahrai, S.M., Mousavi, S.A. and Saatcioglu, M. (2017), "Analytical study on seismic behavior of proposed hybrid tension-only braced frames", *Struct. Design Tall Spec. Build.*, **26**(3), 1-15.

Zhou, Z., He, X.T., Wu, J., Wang, C.L. and Meng, S.P. (2014), "Development of a novel self-centering buckling-restrained brace with BFRP composite tendons", *Steel Comp. Struct., Int. J.*, **16**(5), 491-506.

Zhou, Z., Xie, Q., Lei, X.C., He, X.T. and Meng, S.P. (2015), "Experimental investigation of the hysteretic performance of dual-tube self-centering buckling-restrained braces with composite tendons", *J. Compos. Constr.*, **19**(6), 04015011.

CC